Classical Fractals and Quantum Chaos in Ultracold Dipolar Collisions

B. C. Yang, Jesús Pérez-Ríos, and F. Robicheaux[*]

Department of Physics and Astronomy, Purdue University, West Lafayette, Indiana 47907, USA

We examine a dipolar-gas model to address fundamental issues regarding the correspondence between classical chaos and quantum observations in ultracold dipolar collisions. The theoretical model consists of a short-range Lennard-Jones potential well with an anisotropic, long-range dipole-dipole interaction between two atoms. Both the classical and quantum dynamics are explored for the same Hamiltonian of the system. The classical chaotic scattering is revealed by the fractals developed in the scattering function (defined as the final atom separation as a function of initial conditions), while the quantum chaotic features lead to the repulsion of the eigenphases from the corresponding quantum S matrix. The nearest-eigenphase-spacing statistics have an intermediate behavior between the Poisson and the Wigner-Dyson distributions. The character of the distribution can be controlled by changing an effective Planck constant or the dipole moment. The degree of quantum chaos shows a good correspondence with the overall average of the classical scattering function. The results presented here also provide helpful insights for understanding the role of the inherent dipole-dipole interaction in the currently ongoing experiments on ultracold collisions of highly magnetic atoms.

Anisotropic interactions inherent in ultracold dipolar gases are sources of various exotic phenomena, which have attracted numerous investigations from different perspectives, including those in few-body physics [1–4], ultracold chemistry [5–7], many-body physics [8–14], and quantum computation [15–17]. The recent work on ultracold collisions of highly magnetic atoms like lanthanides has shown a very dense spectrum of Fano-Feshbach resonances [18–20]. The statistics of nearest-neighbor spacings between resonances closely follow the Wigner-Dyson distribution [20], which indicates that the corresponding classical dynamics may be chaotic after the Bohigas-Giannoni-Schmit (BGS) conjecture [21], therefore arousing further interest in quantum chaos of ultracold dipolar collisions [22–28]. The dipole-dipole interaction (DDI), as a typical long-range, anisotropic force, exists universally in dipolar gases [29]. It couples the internal dipole moments with the relative spatial motion between two colliding dipoles, which promises, in principle, a possible complex nonlinear dynamics. However, the recent examination of the Hamiltonian spectral properties concluded that quantum chaotic features observed in ultracold erbium or dysprosium gases originate from a short-range dispersion potential [22] rather than from the long-range DDI.

At the current stage, studies on the DDI-induced dynamics become fundamentally important, and a series of critical questions are awaiting to be resolved on the theoretical side. These questions include (i) whether the classical counterpart has some chaotic features, (ii) if it does, then it means a breakdown of the BGS conjecture, and what the physical origin is, and (iii) for further exploring and understanding the quantum chaos in ultracold dipolar collisions, it is natural and essential to ask how and when

we can expect a certain correspondence between quantum and classical worlds. So far, all reported results are confined to quantum calculations [18,20,22–28], and the classical counterpart is absent.

In this Letter, we directly address the fundamental issues regarding the correspondence between classical chaos and quantum dynamics. Our work is based on a dipolar-gas model without anisotropic dispersion potentials, which represents an effort to understand the role of the inherent DDI in ultracold dipolar collisions instead of reproducing the chaotic spectra as in the experiment [20,22]. We demonstrate that the DDI alone can cause classical chaotic scattering, characterized by fractals in the scattering function $R(\theta_i, t)$, which is defined using the final atom separation R as a function of initially incoming angles θ_i after a time t of propagation. For quantum dynamics, we examine the scattering S matrix instead of spectral properties of the relevant Hamiltonian, because the S matrix is intrinsic to the scattering process and its eigenphases can clearly exhibit the effects of quantum chaotic scattering [30–32]. Using physical parameters adapted from ultracold Er gases, we do not observe an obvious signature of quantum chaos, consistent with previous studies [22]. By appropriately varying an effective Planck constant or the dipole moment, we observe eigenphase repulsion, and a good correspondence is established between the degree of quantum chaos and the overall average of classical scattering function.

The theoretical model consists of two dipoles scattered in a Lennard-Jones potential well $V_0(R)$ [Fig. 1(a)]:

$$H = \frac{\mathbf{p}^2}{2m} + V_0(R) + \frac{C}{R^3}[\mathbf{j}_1 \cdot \mathbf{j}_2 - 3(\mathbf{j}_1 \cdot \hat{\mathbf{R}})(\mathbf{j}_2 \cdot \hat{\mathbf{R}})], \quad (1)$$
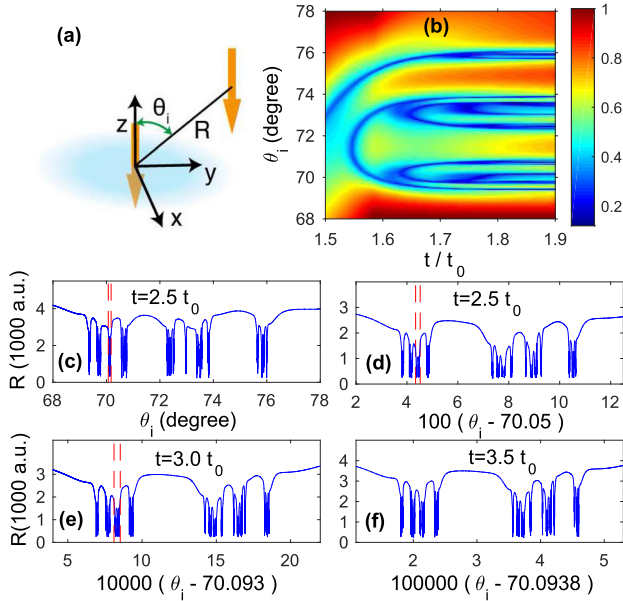
FIG. 1. Schematic model (a) and scattering fractals (b)–(f). (b) Scattering-fractal formation as the propagation time t evolves. The initial distance $R(t = 0)$ between two dipoles is 6000 a.u., and $t_0 = 10^{12}$ a.u. as a time unit. The values of $R(t)$ are indicated by different colors, which have been scaled using the maximum distance value at each time instant. (c)–(f) $R(t)$ as a function of initial angles θ_i, showing the well development of scattering fractals into subtle digits of initial conditions after a long time evolution.

where m and $\mathbf{p}$ are, respectively, the reduced mass and the relative momentum. $V_0(R) = C_{12}/R^{12} - C_6/R^6$ with two adjustable parameters C_{12} and C_6. For clarity, C and $\mathbf{j}_i$ ($i = 1, 2$) are referred to as the dipole-dipole coupling strength and the inherent spin of the colliding dipoles, respectively. For magnetic atoms as in Refs. [20,22], the internal spin $\mathbf{j}$ comes from the total atomic angular momentum. $C = (g\mu_B)^2/c^2$, where g, μ_B, and c denote the atomic g factor, the Bohr magneton, and the speed of light, respectively. Atomic units are used throughout this work unless specified otherwise. The relative spatial motion $(\mathbf{R}, \mathbf{p})$ follows classical Hamiltonian equations, and evolution equations for each spin can be obtained from the classical analog of quantum Ehrenfest equations (see Ref. [33] for an interesting discussion on the classical analog of quantum spin). During the scattering, each dipole moment conserves its amplitude, but its orientation couples with the orbital angular momentum $\mathbf{L} = \mathbf{R} \times \mathbf{p}$ due to the DDI, and the total angular momentum $\mathbf{J} = \mathbf{L} + \mathbf{j}_1 + \mathbf{j}_2$ is conserved. After all the constants of motion are accounted, the classical phase space spanned by $(\mathbf{R}, \mathbf{p}, \mathbf{j}_1, \mathbf{j}_2)$ is reduced to six dimensions.

We assume the two dipoles to be initially along the negative z axis with the same amplitude j [Fig. 1(a)]. The dipoles are generally expected to move around each other when they get close, even if $\mathbf{L}$ is initially zero as in an incoming s wave scattering quantum mechanically.

Depending on the relative angle between $\mathbf{j}(t)$ and $\mathbf{R}(t)$, the anisotropic DDI can be attractive or repulsive, which bounces classical trajectories $\mathbf{R}(t)$ in and out in a complex manner for certain incoming initial angles θ_i relative to the z axis. Figure 1(b) shows the formation of fractals in the classical scattering function $R(\theta_i, t)$ for parameters adapted from ultracold ^{168}Er gases at 400 nK [20], where the two dipoles are started with an incoming radial velocity, i.e., $\mathbf{L} = 0$, with the collision energy determined by the temperature. $C_6 = 1723$ a.u., $j = 6$, $g = 1.164$, and $m = 167.9324/2.0$ amu (also used as a mass unit m_0 hereafter). The value of C_{12} was set to be 8.0783×10^{17} a.u. for convenience. A fourth-order Runge-Kutta algorithm with adaptive time steps was used in propagating trajectories [34]. At each time instant, the scattering function was scaled by its maximum value. The local minima indicated by blue in Fig. 1(b) trace out the formation of scattering fractals with time, and the corresponding trajectories experience a larger number of bounces (between outer and inner turning points each time) than those already escaped. At $t = 1.9t_0$ with $t_0 = 10^{12}$ a.u., the large-scale pattern of fractals forms after a sufficient number of bounces. The remaining trajectories experience more and more bounces as time evolves, and the fractal structure develops into smaller and smaller digits of θ_i, as shown in Figs. 1(c)–1(f), eventually resulting in a high sensitivity of long-time evolution on θ_i in the fractal region and featuring the chaotic scattering dynamics [35–42]. The following discussions will be merged with our efforts in searching the possible imprints of these fractals in quantum dynamics.

Quantum complex systems are customarily studied by assuming some statistical correlations regarding the interactions among numerous states involved in a given basis. It constitutes the basic idea in the random matrix theory (RMT), where the Hamiltonian matrix describing the physical system is assumed to have random entries statistically independent and satisfying a certain transformation criteria. For instance, real symmetric matrices with their entries from a Gaussian orthogonal ensemble are appropriate for a fully chaotic bound system having time-reversal-invariant symmetry [43,44], as in analyzing the Hamiltonian spectra of complex nuclei [45]. On the other hand, the quantum chaotic scattering is usually explored through the corresponding S matrix. For a fully chaotic system, it is preferable to use random unitary symmetric matrices with Dyson's circular orthogonal ensemble (COE) [45–49], which predicts a Wigner-Dyson distribution for the nearest-eigenphase distribution (NED) [46,50]. A physical system may have its S-matrix's eigenphases follow an intermediate statistics between Poisson and Wigner-Dyson distributions. The NED curve can be fitted by [50,51]

$$P(s) = A(\beta)\left(\frac{\pi s}{2}\right)^{\beta} e^{-(\pi^2\beta/16)s^2 - [B(\beta) - (\pi\beta/4)]s}, \quad (2)$$

where β is the Izrailev parameter, indicating the degree of quantum chaos. $A(\beta)$ and $B(\beta)$ are numerically determined

through the relation $\int_0^\infty P(s)ds = \int_0^\infty sP(s)ds = 1$. In Eq. (2), β runs from 0 (Poisson distribution) to 1 (COE) with time-reversal invariance.

We compute the quantum S matrix for our current model in Eq. (1) based on the coupled-channel method described elsewhere [52–54]. Since the total angular momentum $\mathbf{J} = \mathbf{j}_{12} + \mathbf{L}$ and its projection M on the laboratory frame are good quantum numbers, where $\mathbf{j}_{12} = \mathbf{j}_1 + \mathbf{j}_2$, we employ the basis $|j_1j_2j_{12}LJM\rangle$ to solve the corresponding time-independent Schrödinger equation. In our simulations, the scattering occurs from an initially incoming s wave, and the number of channels used is $L_{\max} = 2j_1 + 2j_2$ for a given J and M, guaranteeing that all relevant channels are included. The relevant coupled-channel equations are solved using the hybrid log-derivative-Airy propagator method [55]. The log-derivative propagation starts from 2 a.u. to $R_{\text{swtch}} = 1000$ a.u. with a step size of $0.05/\sqrt{\xi}$ a.u., where ξ denotes the mass factor in units of m_0. For $R > R_{\text{swtch}}$, the Airy propagator takes over with a progressively larger step size with a scaling factor of 1.05. The radial boundary $R_{\max}$ is well in the asymptotic regime, which varies from 6000 to 75 000 a.u., mainly determined by the DDI strength. At $R_{\max}$ the numerical solutions are matched with the asymptotic scattering wave function for computing the S matrix. With these parameters, our simulations are converged to better than 1%.

Our quantum calculations using parameters adapted from ultracold Er gases give no obvious quantum chaotic features, which is the same result as in Ref. [22]. This is in contrast with the classical chaotic scattering revealed in Fig. 1. The absence of quantum-classical correspondence arises from two dynamical differences between quantum and classical mechanics. (a) The classical phase-space structure, like the fractals and chaotic region, can evolve into an arbitrarily small volume, which may be easily washed out as a result of the quantum uncertainty principle, related to the Planck constant $\hbar$. (b) The coupling between internal spins and spatial motion causes a continuous change of the classical angular momentum, but the quantum number of angular momentum and its components can change only by integer intervals. These ideas suggest that the quantum imprints of scattering fractals, as in Fig. 1, could be found by decreasing an effective Planck constant $\tilde{\hbar}$ intrinsic to the corresponding quantum dynamics. For the Hamiltonian in Eq. (1), if we increase the mass m of colliding particles, it is equivalent to decreasing an effective Planck constant according to $\tilde{\hbar} = \hbar\sqrt{m_0/m}$ but keeping $m = m_0$ as for ^{168}Er. On the other hand, a larger spin j also makes the observation of quantum chaos more plausible. Both the smaller $\tilde{\hbar}$ and the larger j values have the same effect, namely, increasing the ratio of the involved classical actions to the relevant Planck constant, which makes quantum dynamics approach the semiclassical limit.

Figure 2 shows the statistics of the quantum S-matrix's NED and its eigenvector distribution for $\tilde{\hbar} = \hbar/\sqrt{1000}$ and $j_1 = j_2 = 12$, with the results for $\tilde{\hbar} = \hbar$ also shown
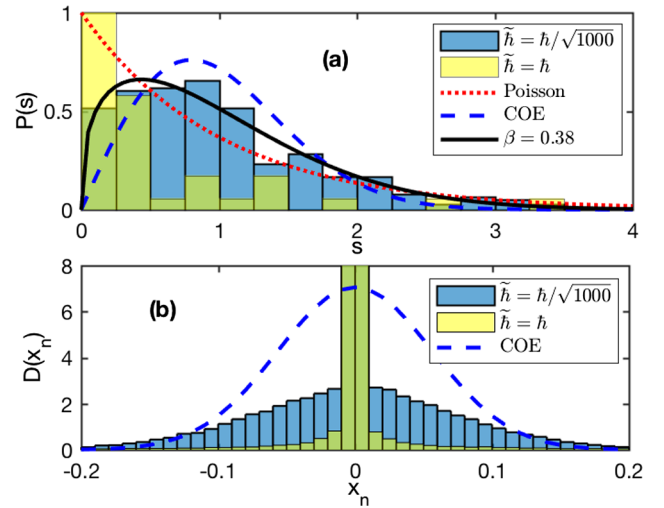

FIG. 2. NED and eigenvector localization of a quantum S matrix for the Hamiltonian in Eq. (1), where $j_1 = j_2 = 12$ at 400 nK. (a) The NED with s in units of the mean spacing π/N. The dotted line, the dashed curve, and the solid black line represent, respectively, the Poisson distribution ($\beta = 0$), the RMT prediction under the COE ($\beta = 1$), and the prediction with $\beta = 0.38$ in Eq. (2). (b) The eigenvector distribution comparing with the COE prediction (dashed curve), where the values of x_n denote the components of all eigenvectors calculated from the S matrix on the basis of $|j_1j_2j_{12}LJM\rangle$. In both (a) and (b), the results for $\tilde{\hbar} = \hbar$ and $\tilde{\hbar} = \hbar/\sqrt{1000}$ are depicted by yellow bars and blue bars, respectively. The green colors are the overlap area between yellow and blue bars.

as a comparison. In Fig. 2(a), the height of the first bin close to zero spacing ($s = 0$) is largely suppressed for $\tilde{\hbar} = \hbar/\sqrt{1000}$, showing a clear eigenphase repulsion. Note that the height of the first bin ($= 2.78$) for $\tilde{\hbar} = \hbar$ is higher than 1, which has been previously observed and identified as the Shnirelman peak [56]. The statistics of the nearest eigenphase spacings for $\tilde{\hbar} = \hbar/\sqrt{1000}$ in Fig. 1(a) show a fairly close behavior to the COE predictions, and the NED curve can be fitted very well using Eq. (2), giving $\beta = 0.38$. In Fig. 2(b), it is clear that the details of eigenvector distributions for $\tilde{\hbar} = \hbar$ are largely different from the COE predictions, echoed by the Shnirelman peak in the eigenphase statistics, while the eigenvector distribution with $\tilde{\hbar} = \hbar/\sqrt{1000}$ is closer to the COE predictions except for a spike near $x_n = 0$, where an effect of eigenvector localization may be involved as discussed in Ref. [50]. These results in Fig. 2, together with Fig. 1, suggest that the classical chaotic region containing scattering fractals occupies a small portion in the whole phase space, and the corresponding quantum-chaotic features could be achieved by scaling the quantum uncertainty degree through an effective Planck constant $\tilde{\hbar}$.

In Fig. 3, we explore the relevant physical parameter space as a systematic inspection of quantum-classical correspondence in the DDI-induced dynamics. Figures 3(a), 3(c), and 3(e) shows the variation of the classical scattering
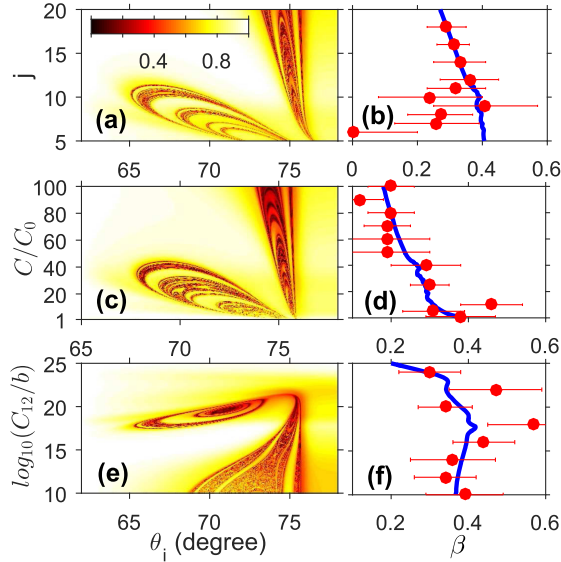
FIG. 3. Quantum-classical correspondence and parameter dependence. (a), (c), and (e) give the relative distances R as a function of θ_i by varying the spin, the DDI strength, and the parameter C_{12}, respectively. The scattering function for each specific parameter has been scaled as in Fig. 1(b), and the heavy colored area indicates the scattering fractal region. C_0 denotes the DDI strength between ^{168}Er atoms. $b = 8.0783$ a.u. Solid points in (b), (d), and (f) represent the calculated β values with error bars at 1σ standard deviation. Solid lines give the classical global quantity ϖ defined from the overall average of the classical scattering function, which was shifted by an arbitrary constant to compare with the β values.

function $[R(t) \text{ vs } \theta_i]$ with the parameters j, C, and C_{12}, respectively. The quantum calculations with an effective Planck constant $\tilde{\hbar} = \hbar/\sqrt{1000}$ are presented by the solid points in Figs. 3(b), 3(d), and 3(f), using the fitted β value in Eq. (2) as an indicator for the degree of quantum chaos. $j = 12$ in Figs. 3(c)–3(f). The values of C_{12} and C are the same as in Fig. 1 if not being varied in Fig. 3. All of the classical results were calculated after the large-scale fractals already formed as in Fig. 1(b), and the initially incoming distance was chosen in the asymptotic regime. Specifically, we used $R(t = 0) = 15\,000$ a.u. and $t = 5t_0$ for Fig. 3(a), $R(t = 0) = 80\,000$ a.u. and $t = 24t_0$ for Fig. 3(c), and $R(t = 0) = 10\,000$ a.u. and $t = 3.5t_0$ for Fig. 3(e). The scattering fractals are sketched by the heavy colored area, which shows complex but interesting structures. Our calculations show that much richer leaf structures can further develop out, for example, by decreasing C_{12} in Fig. 3(c) or increasing the C value in Fig. 3(e).

To compare with the quantum results quantitatively, we use an overall average of classical scattering function, i.e., the average distance $\bar{R}$ of 10^4 trajectories initially launched on the uniform grid in $\cos(\theta_i)$ from 0 to 1, to define a global variable $\varpi = 1 - \bar{R}/\bar{R}_{\max}$ with $\bar{R}_{\max}$ denoting the maximum value of $\bar{R}$ in the full parameter range explored. This global quantity represents an averaged relative trapping distance,

related to the trapped trajectories in fractal basins. A larger ϖ indicates that more scattering trajectories are trapped in a short distance between the two colliding dipoles. As demonstrated in Figs. 3(b), 3(d), and 3(f), the classical ϖ values display a very similar behavior in the parameter space as the quantum β values. This agreement is somewhat surprising but clearly reveals a certain correspondence between classical and quantum dynamics, which requires more work and insights in the future. From Fig. 3, at least three immediate observations can be reached as follows. First, both the classical and quantum dynamics display a nontrivial parameter dependence. In particular, the DDI-induced dynamics does not simply become more chaotic by increasing the internal dipole moment, the DDI strength, or the potential-well depth. Second, the degree of quantum chaos is generally suppressed for sufficiently small spins [Fig. 3(b)], though the corresponding classical dynamics exhibits obvious chaotic scattering. Furthermore, there is a fluctuation observed in β values around the classical averaged curve, especially in Fig. 3(f), which is partly associated with the scaling-invariant symmetry of the Hamiltonian in Eq. (1). Our preliminary examination shows that the classical scattering function experiences only a subtle change by varying C and j simultaneously but keeping their product Cj^2 constant, and the classical curve as in Fig. 3(f) is almost unchanged. However, the quantum calculations as in Fig. 2 is more sensitive to the specific C and j values individually.

In summary, we have explored the DDI-induced dynamics from both the classical and quantum viewpoints. Based on a dipolar-gas model, the classical counterpart of quantum dynamics has been studied for the first time, where the embedded classical chaotic scattering has been confirmed by the universal existence of scattering fractals. The signature of quantum chaos has been examined in the eigenphase statistics of the quantum S matrix, which represents an alternative and straightforward perspective beyond existing studies on the Hamiltonian spectral properties [22–28]. It has been shown that, for a sufficiently large dipole moment and a relatively small effective Planck constant, a good correspondence can be established between the degree of quantum chaos and an overall average of the classical scattering function; otherwise, the observed degree of quantum chaos is largely suppressed. This direct correspondence provides further insights beyond the Berry-Robnik semiclassical picture [57,58] in understanding the first-principles connections between classical chaotic scattering and quantum observations, especially with the coupling between internal degrees of freedom and the external dynamics.

The results presented here open a possible way to understand the role of the inherent DDI in ultracold dipolar collisions. These ideas hold important implications for understanding the complex chaotic scattering in the currently ongoing experiments [20,22] and also provide valuable insights for future investigations on the quantum chaos in ultracold dipolar gases. Following our current model study, more realistic consideration by including an additional

dispersion potential is in progress. Generalizations to many other practical situations are also expected, such as collisions of magnetic dipoles in an external magnetic field, as well as the electric dipolar scattering between polar molecules.

————————

[*]robichf@purdue.edu

[1] J. L. Bohn, M. Cavagnero, and C. Ticknor, New J. Phys. **11**, 055039 (2009).

[2] Y. Wang, J. P. D'Incao, and C. H. Greene, Phys. Rev. Lett. **107**, 233201 (2011).

[3] M. Mayle, B. P. Ruzic, and J. L. Bohn, Phys. Rev. A **85**, 062712 (2012).

[4] J. F. E. Croft and J. L. Bohn, Phys. Rev. A **89**, 012714 (2014).

[5] G. Quéméner and P. S. Julien, Chem. Rev. **112**, 4949 (2012).

[6] M. H. G. de Miranda, A. Chotia, B. Neyenhuis, D. Wang, G. Quéméner, S. Ospelkaus, J. L. Bohn, J. Ye, and D. S. Jin, Nat. Phys. **7**, 502 (2011).

[7] J. Pérez-Ríos, M. Lepers, R. Vixeau, N. Bouloufa-Maafa, and O. Dulieu, J. Phys. Conf. Ser. **488**, 012031 (2014).

[8] M. A. Baranov, M. Dalmonte, G. Pupillo, and P. Zoller, Chem. Rev. **112**, 5012 (2012).

[9] T. Lahaye, J. Metz, B. Fröhlich, T. Koch, M. Meister, A. Griesmaier, T. Pfau, H. Saito, Y. Kawaguchi, and M. Ueda, Phys. Rev. Lett. **101**, 080401 (2008).

[10] L. Santos, G. V. Shlyapnikov, and M. Lewenstein, Phys. Rev. Lett. **90**, 250403 (2003).

[11] S. Ronen, D. C. E. Bortolotti, and J. L. Bohn, Phys. Rev. Lett. **98**, 030406 (2007).

[12] K.-K. Ni, S. Ospelkaus, D. Wang, G. Quéméner, B. Neyenhuis, M. H. G. de Miranda, J. L. Bohn, J. Ye, and D. S. Jin, Nature (London) **464**, 1324 (2010).

[13] H. Kadau, M. Schmitt, M. Wenzel, C. Wink, T. Maier, I. Ferrier-Barbut, and T. Pfau, Nature (London) **530**, 194 (2016).

[14] B. Gadway and B. Yan, J. Phys. B **49**, 152002 (2016).

[15] D. DeMille, Phys. Rev. Lett. **88**, 067901 (2002).

[16] S. F. Yelin, K. Kirby, and R. Côté, Phys. Rev. A **74**, 050301 (R) (2006).

[17] L. D. Carr, D. DeMille, R. V. Krems, and J. Ye, New J. Phys. **11**, 055049 (2009).

[18] A. Petrov, E. Tiesinga, and S. Kotochigova, Phys. Rev. Lett. **109**, 103002 (2012).

[19] K. Baumann, N. Q. Burdick, M. Lu, and B. L. Lev, Phys. Rev. A **89**, 020701(R) (2014).

[20] A. Frish, M. Mark, K. Aikawa, F. Ferlaino, J. L. Bohn, C. Makrides, A. Petrov, and S. Kotochigova, Nature (London) **507**, 475 (2014).

[21] O. Bohigas, M. J. Giannoni, and C. Schmit, Phys. Rev. Lett. **52**, 1 (1984).

[22] T. Maier *et al.*, Phys. Rev. X **5**, 041029 (2015).

[23] K. Jachymski and P. S. Julienne, Phys. Rev. A **92**, 020702 (R) (2015).

[24] T. Maier, I. Ferrier-Barbut, H. Kadau, M. Schmitt, M. Wenzel, C. Wink, T. Pfau, K. Jachymski, and P. S. Julienne, Phys. Rev. A **92**, 060702(R) (2015).

[25] M. L. González-Martínez and P. S. Żuchowski, Phys. Rev. A **92**, 022708 (2015).

[26] J. Mur-Petit and R. A. Molina, Phys. Rev. E **92**, 042906 (2015).

[27] D. G. Green, C. L. Vaillant, M. D. Frye, M. Morita, and J. M. Hutson, Phys. Rev. A **93**, 022703 (2016).

[28] M. D. Frye, M. Morita, C. L. Vaillant, D. G. Green, and J. M. Hutson, Phys. Rev. A **93**, 052713 (2016).

[29] T. Lahaye, C. Menotti, L. Santos, M. Lewenstein, and T. Pfau, Rep. Prog. Phys. **72**, 126401 (2009).

[30] R. Blümel and U. Smilansky, Physica (Amsterdam) **36D**, 111 (1989).

[31] R. Blümel and U. Smilansky, Phys. Rev. Lett. **60**, 477 (1988).

[32] R. Blümel and U. Smilansky, Phys. Rev. Lett. **64**, 241 (1990).

[33] A. O. Barut, M. Bozic, and Z. Maric, Ann. Phys. (N.Y.) **214**, 53 (1992).

[34] W. H. Press, M. R. Flannery, S. A. Teukolsky, and W. T. Vetterling, *Numerical Recipes in C* (Cambridge Univeristy Press, Cambridge, England, 1988).

[35] D. W. Noid, S. K. Gray, and S. A. Rice, J. Chem. Phys. **84**, 2649 (1986).

[36] B. K. Balasubramanian, A. Mishra, S. Bahel, S. Kumar, and N. Sathyamurthy, J. Chem. Phys. **95**, 4160 (1991).

[37] S. Mahpatra, R. Ramaswamy, and N. Sathyamurthy, J. Chem. Phys. **104**, 3989 (1996).

[38] K. A. Mitchell, J. P. Handley, B. Tighe, A. Flower, and J. B. Delos, Phys. Rev. Lett. **92**, 073001 (2004).

[39] K. A. Mitchell and J. B. Delos, Physica (Amsterdam) **229D**, 9 (2007).

[40] P. Hansen, K. A. Mitchell, and J. B. Delos, Phys. Rev. E **73**, 066226 (2006).

[41] J. Novick, M. L. Keeler, J. Giefer, and J. B. Delos, Phys. Rev. E **85**, 016205 (2012).

[42] J. Novick and J. B. Delos, Phys. Rev. E **85**, 016206 (2012).

[43] E. P. Wigner, Ann. Math. **62**, 548 (1955).

[44] E. P. Wigner, Ann. Math. **65**, 203 (1957).

[45] M. L. Mehta, *Random Matrices and the Statistical Theory of Energy Levels* (Academic, New York, 1967).

[46] F. J. Dyson, J. Math. Phys. (N.Y.) **3**, 140 (1962).

[47] F. J. Dyson, J. Math. Phys. (N.Y.) **3**, 157 (1962).

[48] F. J. Dyson, J. Math. Phys. (N.Y.) **3**, 166 (1962).

[49] F. J. Dyson, J. Math. Phys. (N.Y.) **3**, 1191 (1962).

[50] F. M. Izrailev, Phys. Rep. **196**, 299 (1990).

[51] R. Scharf and F. M. Izrailev, J. Phys. A **23**, 963 (1990).

[52] T. V. Tscherbul, Y. V. Suleimanov, V. Aquilanti, and R. V. Krems, New J. Phys. **11**, 055021 (2009).

[53] J. Pérez-Ríos, M. Bartolomei, J. Campos-Martínez, M. I. Hernández, and R. Hernández-Lamoneda, J. Phys. Chem. A **113**, 14952 (2009).

[54] J. Pérez-Ríos, J. Campos-Martínez, and M. I. Hernández, J. Chem. Phys. **134**, 124310 (2011).

[55] M. H. Alexander and D. E. Manolopoulos, J. Chem. Phys. **86**, 2044 (1987).

[56] B. V. Chirikov and D. L. Shepelyansky, Phys. Rev. Lett. **74**, 518 (1995).

[57] M. V. Berry and M. Robnik, J. Phys. A **17**, 2413 (1984).

[58] M. Robnik, J. Phys. A **20**, L495 (1987).